The Importance of the Surface Divergence Term in the Finite Element-Vector Absorbing Boundary Condition Method

Vassilios N. Kanellopoulos and J. P. Webb

Abstract—**The vector absorbing boundary condition (ABC) is an effective way of truncating the infinite domain of a 3-D scattering problem, and thereby permitting its solution with a finite element method. One of the terms of the ABC is a surface divergence term. It is shown that due to its presence, the normal continuity of the field must be enforced on the surface where the ABC is applied. Numerical analysis of scattering by a conducting sphere demonstrates that if normal continuity is not enforced, the maximum error in the near field may more than double. A similar error occurs if the surface divergence term is omitted from the formulation.**

I. Introduction

The advantage of partial differential equation techniques like the finite element method (FEM) or the finite difference method (FDM) over other methods is that they can handle highly inhomogeneous materials and arbitrarily shaped objects without any extra effort in the computer code regarding material interfaces. These techniques can be used to solve open boundary vector wave problems (i.e., electromagnetic scattering) if proper boundary conditions are applied on an external surface that truncates the exterior infinite volume and completely encloses the discretized volume of interest, V. These boundary conditions may be global or local in nature. Global boundary conditions, like the integral equation condition (IEC) [2] are exact, but they produce full matrices, destroying the sparsity of the FEM or FDM. This is a disadvantage in memory efficiency and computational costs. Local boundary conditions such as the absorbing boundary conditions (ABC's) lead to sparse matrices [1]. The ABC's are approximate, and higher order ABC's absorb better than lower order ones.

The ABC's can be symmetric or nonsymmetric, depending on the type of matrix they produce. Symmetric matrices are preferred because: a) they require considerably less computer memory (only half of the final matrix needs to be stored) and b) the more efficient symmetric solvers can be used for the solution of the matrix equation. Symmetric ABC's can also be included in variational formulations of the finite element method (FEM).

Symmetric vector ABC's were first developed in 1989 [3], and they were successfully implemented and tested in 3-D vector wave problems [4]–[6]. It was shown that when the second order ABC is applied on the outer spherical absorbing boundary surface (ABS), high accuracy can be obtained (average error in the near field less than 1%) by placing the ABS no more than 0.3 wavelengths away from the scatterers. Recent work showed the possibility that the ABS may not be a sphere, but a rather more conformal surface to the scatterers [7]–[8].

Manuscript received September 26, 1994; revised May 25, 1995.

V. N. Kanellopoulos is with the Telecommunications Division, Electrical Engineering Department, Aristotle University of Thessaloniki, GR-540 06 Thessaloniki, Greece.

J. P. Webb is with the Computational Analysis and Design Laboratory, Electrical Engineering Department, McGill University, Montréal, Québec, H3A 2A7 Canada.

IEEE Log Number 9413408.

For the second order ABC, the following functional is stationary with respect to the magnetic field

$$F(\mathbf{H}^s) = \int_V \{(\nabla \times \mathbf{H}^s)^2 - k_0^2 H^{s^2}\}\, dV + \int_S \{\alpha \mathbf{H}_t^{s^2} + \beta(r)[\hat{\mathbf{a}}_r \cdot (\nabla \times \mathbf{H}^s)]^2 - \beta(r)(\nabla \cdot \mathbf{H}_t^s)^2\}\, dS \quad (1)$$

where $\mathbf{H}^s$ is the unknown scattered complex vector magnetic field, V is the volume of interest, S is the spherical ABS, $k_0 = \omega\sqrt{\epsilon_0 \mu_0}$ is the free-space wavenumber, $\hat{\mathbf{a}}_r$ is the radial unit vector, $\alpha = jk_0$ and $\beta = 1/(2jk_0 + 2/r)$. The subscript t denotes the component tangential to the ABS.

The second order ABC implemented above is approximate, valid for outward-propagating waves and improves at a rate of r^{-5} [3], [9]. It is characterized by three terms, the last of which is the surface divergence term. If edge elements are used, so that only tangential continuity but not normal continuity is imposed on the vector field in the FE discretization [10], the first two terms can be modeled in a straightforward manner. However, the surface divergence term requires more continuity than edge elements provide, and if this is not taken into account, erroneous results may occur. These are discussed in detail in the next section. Perhaps because of the extra difficulties caused by the surface divergence term, it has been suggested that it should be omitted altogether. The results presented here confirm that the divergence term, when properly implemented, can substantially improve the accuracy of the computed field.

II. The Surface Divergence Term

In this work the covariant projection element, a type of edge element, was used [11]. It is a curvilinear hexahedron and uses mixed order trial functions (first and second order) for the field.

Dividing the volume of interest into M covariant projection elements, using [(19) p. 501] and [(42) p. 503 in [12]], and after some algebra, the first variation of the functional F (1) gives

$$\begin{aligned}
&\frac{1}{2}\delta(F(\mathbf{H}^s)) \\
&= \sum_{i=1}^{M} \int_{V_i} \delta\mathbf{H}^s \cdot [\nabla \times \nabla \times \mathbf{H}^s - k_0^2 \mathbf{H}^s]\, dV \\
&\quad + \sum_{j=1}^{N} \int_{Q_j} \delta\mathbf{H}^s \cdot \{\nabla \times \mathbf{H}^s \times \hat{\mathbf{a}}_r + \alpha \mathbf{H}_t^s + \beta(r)\nabla_t(\nabla \cdot \mathbf{H}_t^s) \\
&\quad + \beta(r)\nabla \times \hat{\mathbf{a}}_r[\hat{\mathbf{a}}_r \cdot (\nabla \times \mathbf{H}^s)]\}\, dS \\
&\quad + \sum_{k=1}^{L} \beta(r) \int_{C_k}^{l} \hat{\mathbf{a}}_m^l \cdot \{\delta\mathbf{H}_t^s \nabla \cdot \mathbf{H}_t^s + \delta\mathbf{H}^s \\
&\quad \times \hat{\mathbf{a}}_r[\hat{\mathbf{a}}_r \cdot (\nabla \times \mathbf{H}^s)]\}\, dC \\
&\quad + \sum_{c=1}^{L_c} \beta(r) \int_{C_c}^{r} \hat{\mathbf{a}}_m^r \cdot \{\delta\mathbf{H}_t^s \nabla \cdot \mathbf{H}_t^s + \delta\mathbf{H}^s \\
&\quad \times \hat{\mathbf{a}}_r[\hat{\mathbf{a}}_r \cdot (\nabla \times \mathbf{H}^s)]\}\, dC \qquad (2)
\end{aligned}$$

where V_i is the subvolume of the ith finite element, Q_j is the surface of the jth quadrilateral on the ABS, N is the total number of curvilinear quadrilaterals the ABS is divided into, C_k is the kth edge on the ABS, L is the total number of edges on the ABS, C_c is the cth common edge on the ABS (i.e., shared by two quadrilaterals), and L_c is the total number of common edges on the ABS, see Fig. 1. $L_c \leq L$. The superscript l denotes the left and the r the right quadrilateral sharing C_c, see also Fig. 1. $\hat{\mathbf{a}}_m^l$ is the unit vector in the

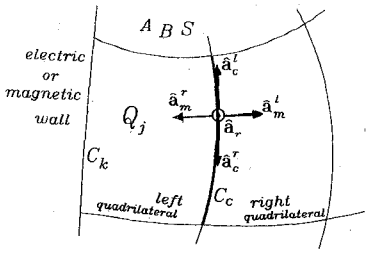

Fig. 1. The quadrilateral Q_j lies on the absorbing boundary surface, ABS and is one of the six faces of the curvilinear covariant projection element that touches the ABS. The edge C_c on the ABS is shared by two quadrilaterals, while the edge C_k is not shared and it touches an electric or magnetic wall. $\hat{\mathbf{a}}_r$, $\hat{\mathbf{a}}_m^l$, $\hat{\mathbf{a}}_m^r$, $\hat{\mathbf{a}}_c^l$, $\hat{\mathbf{a}}_c^r$, $\hat{\mathbf{a}}_c^l$ and $\hat{\mathbf{a}}_c^r$ are the unit vectors.

plane tangent to the ABS and perpendicular to C_c, and $\hat{\mathbf{a}}_m^l = -\hat{\mathbf{a}}_m^r$. At the stationary point of $\boldsymbol{F}$, $\delta(\boldsymbol{F}) = 0$ for every $\delta\mathbf{H}^s$, and we have

$$\nabla \times \nabla \times \mathbf{H}^s - k_0^2 \mathbf{H}^s = 0 \tag{3}$$

$$\nabla \times \mathbf{H}^s \times \hat{\mathbf{a}}_r + \alpha(r)\mathbf{H}_t^s + \beta(r)\{\nabla_t(\nabla \cdot \mathbf{H}_t^s) + \nabla \times \hat{\mathbf{a}}_r[\hat{\mathbf{a}}_r \cdot (\nabla \times \mathbf{H}^s)]\} = 0 \tag{4}$$

and

$$\sum_{k=1}^{L} \beta(r) \int_{C_k}^{l} \{\hat{\mathbf{a}}_m^l \cdot \delta\mathbf{H}_t^s \nabla \cdot \mathbf{H}_t^s + \hat{\mathbf{a}}_c^l \cdot \delta\mathbf{H}_t^s[\hat{\mathbf{a}}_r \cdot (\nabla \times \mathbf{H}^s)]\}\, dC + \sum_{c=1}^{L_c} \beta(r) \int_{C_c}^{r} \{\hat{\mathbf{a}}_m^r \cdot \delta\mathbf{H}_t^s \nabla \cdot \mathbf{H}_t^s + \hat{\mathbf{a}}_c^r \cdot \delta\mathbf{H}_t^s[\hat{\mathbf{a}}_r \cdot (\nabla \times \mathbf{H}^s)]\}\, dC = 0. \tag{5}$$

Equation (3) is the governing curl-curl equation in volume V, and in each sub-volume V_i. Similarly for (4) which is the second order absorbing boundary condition applied on the ABS and consequently on each quadrilateral Q_j. In (5) $\hat{\mathbf{a}}_c^l$ is the unit vector in the plane tangent to the ABS, and tangential to C_c, and $\hat{\mathbf{a}}_c^l = -\mathbf{a}_c^r$, see Fig. 1. Note that $\mathbf{H}_t^s$ denotes the field tangent to the spherical surface S, rather than the field tangent to C_c.

The first variation of the functional (2) will vanish if and only if the sum of the two line integrals on each common edge C_c (5) is zero on the ABS. Since the tangential field continuity is imposed, $\hat{\mathbf{a}}_c^l \cdot \delta\mathbf{H}_t^s = -\hat{\mathbf{a}}_c^r \cdot \delta\mathbf{H}_t^s$, and the vanishing of the first variation just enforces the continuity of $\hat{\mathbf{a}}_r \cdot (\nabla \times \mathbf{H}^s)$, which is correct. However, normal field continuity is not imposed, and requiring that the first variation of the functional vanishes forces $\nabla \cdot \mathbf{H}_t^s = 0$ on both sides of the line, a restriction which is in general wrong, because in the air we have

$$\nabla \cdot \mathbf{H}^s = 0 \Rightarrow \nabla \cdot \mathbf{H}_t^s = -\frac{1}{r^2}\frac{\partial}{\partial r}(r^2 H_r^s) \neq 0. \tag{6}$$

To correct this, $\hat{\mathbf{a}}_m^l \cdot \delta\mathbf{H}_t^s = -\hat{\mathbf{a}}_m^r \cdot \delta\mathbf{H}_t^s$ has to be enforced, i.e., normal continuity across quadrilaterals on the field components tangent to the ABS. This imposes continuity of $\nabla \cdot \mathbf{H}_t^s$ which (from (6)) is correct.

Suppose now that C_k lies on a magnetic wall, i.e., it is the intersection of the ABS and a magnetic wall. It is assumed that the ABS and the wall are perpendicular. In this case, there is only one line integral along C_k (from the left quadrilateral) and $\hat{\mathbf{a}}_c^l \cdot \delta\mathbf{H}_t^s = 0$ is imposed explicitly because of the magnetic wall. Then (5) implies $\nabla \cdot \mathbf{H}_t^s = 0$. Since H_r^s and $\frac{\partial H_r^s}{\partial r}$ are set to zero on the magnetic wall, it can be seen from (6) that this is correct.

Suppose now that C_k lies on an electric wall, i.e. it is the intersection of the ABS and an electric wall. Again, there is only one line integral along C_k, and it is assumed that the ABS and the wall are perpendicular. Then, in order for (5) to be satisfied, it is necessary that $\nabla \cdot \mathbf{H}_t^s = 0$ and $\hat{\mathbf{a}}_r \cdot (\nabla \times \mathbf{H}^s) = 0$ on C_k. The latter condition is equivalent to $E_r^s = 0$ on C_k which is correct (due to the electric wall). The first condition, however, imposes something which is untrue. Thus, in order to have the right boundary conditions, we need to explicitly impose $\hat{\mathbf{a}}_m^l \cdot \delta\mathbf{H}_t^s = 0$ on C_k on magnetic walls.

The analysis for the functional for the electric field is almost identical: it is only necessary to replace $\boldsymbol{H}$ by $\boldsymbol{E}$ and interchange "magnetic wall" and "electric wall" in the above.

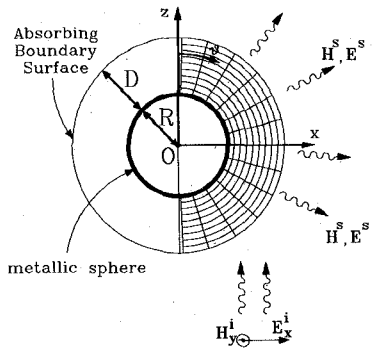

Fig. 2. A x-z cross section of the 3-D geometry. The metallic sphere of radius R has its center at the origin O. It is completely enclosed by a concentric sphere, the ABS, of radius $R + D$. The incident plane wave is x-polarized and z-traveling. Due to symmetries only one-fourth of the region was modeled with curvilinear covariant projection finite elements.

III. Results

The problem of the metallic sphere scatterer in the presence of an incident plane wave was solved numerically in order to investigate and confirm the proposed theory. The geometry of the problem is shown in Fig. 2. The incident plane was x-polarized and z-traveling, and the metallic sphere had its center at $(x, y, z) = (0, 0, 0)$. Due to symmetries, only one quarter of the volume was modeled with the following boundary conditions (see also Fig. 2): $r = R = 0.3\lambda$ (prescribed H_θ^s and H_ϕ^s), $\theta = 3°$ and $\theta = 177°$ (prescribed H_r^s and H_ϕ^s) were the excitation surfaces, $r = R + D$ the ABS, and $\phi = 0°$ and $\phi = 90°$ were the magnetic and the electric walls, respectively.

There were twelve and six elements in the θ and ϕ directions, respectively, and one element every 0.03λ in the r direction, where λ is the wavelength, see Fig. 2. The size of each curvilinear element was $(r, \theta, \phi) = (0.03\lambda, 14.5°, 15°)$. Since H_θ and H_ϕ are undefined on the z-axis, the z-axis was not modeled.

The problem was solved in four different cases:

1) The second order ABC was used and the normal field continuity was enforced on the ABS.
2) The second order ABC was used but the normal field continuity was not enforced on the ABS.
3) An incomplete second order ABC was used that omitted the surface divergence term, and the normal field continuity was not enforced on the ABS.
4) An incomplete second order ABC was used that omitted the surface divergence term, but the normal field continuity was enforced on the ABS.

The results in cases 3) and 4) was almost identical, and therefore, results for case 4) are not shown. Mathematical details on how the normal field continuity was enforced on the ABS may be found in [9]. The computed FE results were compared with analytical solutions found in [13], [5]. The maximum field error shown in Fig. 3 is the largest value of

$$e = |\mathbf{H}_{\text{FEM}}^s - \mathbf{H}_{\text{analytical}}^s|$$

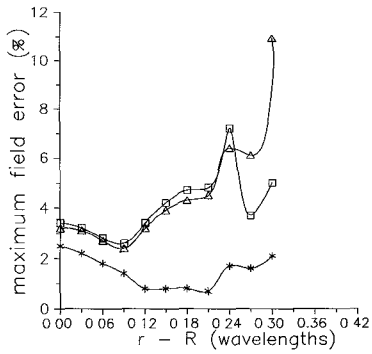

Fig. 3. Solution error versus r-R which is the distance from the metallic sphere scatterer. The radius of the metallic sphere is $R = 0.3\lambda$, and $D = 0.3\lambda$. The stars show the error using the complete form of the second order vector ABC and enforcing normal field continuity on the ABS. The triangles show the error when normal continuity has not been enforced on the ABS, and the squares show the error when in addition to the absence of the normal continuity enforcement, the surface divergence term was absent from the functional.

over the volume modeled, expressed as a percentage of $|\mathbf{H}^s_{\text{analytical}}|$ at the point where the largest value of e occurs. Fine meshes were used so that the discretization errors were reduced to a minimum.

Fig. 3 show the errors for the cases 1), 2), and 3), when $D = 0.3\lambda$. It is clear that in case a) the results are far more accurate than those in cases 2) and 3). In fact, cases 2) and 3) appear to give about the same accuracy in the computed field.

IV. Conclusion

Due to the presence of the surface divergence term, the proper implementation of the second order absorbing boundary condition requires that the two extra conditions be explicitly enforced:

1) On the ABS, normal continuity has to be imposed between the quadrilaterals the ABS is divided into;
2) for the magnetic field case, where the ABS meets an electric wall, the component of magnetic field normal to the wall must be set to zero explicitly; for the electric field case, where the ABS meets a magnetic wall, the component of electric field normal to the wall must be set to zero explicitly.

Numerical results confirm the theory. If the second order ABC is to be used, then the two above conditions are necessary. If they are not imposed, then the error in the near field increases by a factor of at least two. In addition, if these two conditions are not imposed, the numerical results showed that the surface divergence term might as well be dropped out from the formulation.

Acknowledgment

The authors are grateful to Prof. T. D. Tsiboukis for his help and kind support, and to the Electrical Engineering Department (Telecommunications Division) of Aristotle University of Thessaloniki for using its facilities.

References

[1] A. F. Peterson, "Absorbing boundary conditions for the vector wave equation," *Microwave and Optical Technol. Lett.*, vol. 1, no. 2, pp. 62–64, Apr. 1988.

[2] J. M. Jin and J. L. Volakis, "A finite element-boundary integral formulation for scattering by three-dimensional cavity-backed apertures," *IEEE Trans. Antennas Propagat.*, 39, no. 1, pp. 97–104, Jan. 1991.

[3] J. P. Webb and V. N. Kanellopoulos, "Absorbing boundary conditions for the finite element solution of the vector wave equation," *Microwave and Optical Technol. Lett.*, vol. 2, no. 10, pp. 370–372, Oct. 1989.

[4] ——, "A numerical study of vector absorbing boundary conditions for the finite-element solution of Maxwell's equations," *IEEE Microwave and Guided Wave Lett.*, vol. 1, no. 11, pp. 325–327, Nov. 1991.

[5] ——, "3-D finite element analysis of a metallic sphere scatterer: Comparison of first and second order vector absorbing boundary conditions," *Journal de Physique III France 3*, pp. 563–572, Mar. 1993.

[6] ——, "Modeling the electromagnetic field in lossy dielectrics using finite elements and vector absorbing boundary conditions," *IEEE Trans. Microwave Theory and Tech.*, vol. 43, no. 4, pp. 823–827, Apr. 1995.

[7] A. Chatterjee, J. M. Jin, and J. L. Volakis, "Edge-Based Finite Elements and Vector ABC's Applied to 3-D Scattering," *IEEE Trans. Antennas Propagat.*, 41, no. 2, pp. 221–226, Feb. 1993.

[8] A. Chatterjee and J. L. Volakis, "Conformal absorbing boundary conditions for the vector wave equation," *Microwave and Opt. Technol. Lett.*, vol. 6, no. 16, pp. 886–889, Dec. 1993.

[9] V. N. Kanellopoulos, "Finite elements and vector absorbing boundary conditions in 3-D," Ph.D. Thesis, McGill Univ., Montréal, Canada, 1991.

[10] J. P. Webb, "Edge Elements and what they can do for you," *IEEE Trans. Magnetics*, 29, no. 2, pp. 1460–1465, Mar. 1993.

[11] C. Crowley, P. P. Silvester, and H. Hurwitz, Jr., "Covariant projection elements for 3-D vector field problems," *IEEE Trans. Magnetics*, 24, no. 1, pp. 397–400, Jan. 1988.

[12] J. Van Bladel, *Electromagnetic Fields*. New York: McGraw-Hill, 1964.

[13] R. F. Harrington, *Time-Harmonic Electromagnetic. Fields* New York: McGraw-Hill, 1961.

Coupling of the PISCES Device Modeler to a 3-D Maxwell FDTD Solver

Vincent A. Thomas, Michael E. Jones, and Rodney J. Mason

***Abstract*—We show how PISCES-like semiconductor models can be joined non-invasively to finite difference time domain models for the calculation of coupled external electromagnetics. The method involves "tricking" the standard current boundary condition for the device model into accepting an effective parallel external capacitance. For nearly steady state device conditions we show the results for a transmission line-coupled PISCES diode to agree well with those for an ideal diode.**

I. Introduction

The FDTD method advances Maxwell's equations in time on a finite difference mesh [1]. It is being used increasingly to analyze microwave circuits. Sui *et al.* [2] have shown how it might be extended to systems including active elements. Also, two of us recently demonstrated a technique [3] for robustly coupling FDTD to SPICE [4] circuit simulators for subgrid scale modeling. The present note extends this technique to provide coupling noninvasively of FDTD to the PISCES [5] device modeler. We demonstrate this procedure with application to a diode fixed to the end of a transmission line.

Manuscript received September 29, 1994; revised February 15, 1995. This work was supported in part by a cooperative research agreement between Cray Research, Inc. and the Los Alamos National Laboratory.

The authors are with the Los Alamos National Laboratory, Los Alamos, NM 87545 USA.

IEEE Log Number 9413409.